


# Position Analysis of the Atomiser Unit of an Aerosol-on-Demand Jet-Printhead by means of Computational Fluid Dynamics

Martin Ungerer, Tim P. Walter and Ingo Sieber<sup>a</sup>

*Institute for Automation and Applied Informatics, KIT, Hermann-von-Helmholtz-Platz 1,  
76344 Eggenstein-Leopoldshafen, Germany*

**Keywords:** Computational Fluid Dynamics, Modelling, Simulation, Tolerancing, Additive Manufacturing, Aerosol-on-Demand.

**Abstract:** In this paper we present position analysis of the atomiser unit of a newly developed concept of a printhead for Aerosol-on-Demand (AoD) jet-printing using fluid dynamical modelling and simulation. In our concept of the AoD printhead, the ink is atomised by ultrasonic excitation and focussed by a sheath gas in a converging nozzle. Critical for the functioning of the AoD printing process is a proper positioning of the atomiser unit inside the printhead. Using computational fluid dynamics (CFD), we present a position analysis of the atomiser unit with respect to axial misalignment and tilting.

## 1 INTRODUCTION


Printing processes have been discussed for a few decades with regard to their potential applications for additive manufacturing of electronics, also referred to as printed electronics (PE) or functional printing (Cui 2016; Gengenbach et al. 2020). In contrast to conventional, subtractive processes for electronics fabrication, PE enables an optimised material usage and thus less waste (Dyson 2022). Inks that contain functional dielectrics, semiconducting or conducting materials are printed onto a substrate in layers according to the structure of the component to be realised (Cui 2016). Moreover, printing of functional inks offers new opportunities for the realisation of novel devices and systems with special physical, optical, or chemical properties (Siringhaus and Shimoda 2003; Sieber, Thelen, and Gengenbach 2020, 2021; Magdassi 2010).

Besides conventional, contact-based techniques such as gravure-printing and screen-printing that need printing forms for the ink transfer, also digital, contactless processes are used in PE (Zikulnig et al. 2023). Among the digital printing techniques, piezo inkjet is considered the most important principle. It has already reached the necessary maturity for industrial use, but it is limited in terms of ink viscosity

and resolution (Kwon et al. 2020). To overcome these limitations, other technologies such as aerosol jet printing (AJP) and electrohydrodynamic jet are being developed (Cui 2016; Kwon et al. 2020). However, electrohydrodynamic jet as well as inkjet still face some challenges with regard to printing on non-planar substrates (Kwon et al. 2020; Oakley and Chahal 2018).

Aerosol jet printing (AJP) is a promising process in the field of functional printing of new materials, especially nanomaterial-loaded inks (Ganz et al. 2016; Gupta et al. 2016). In contrast to the inkjet process, AJP offers higher resolution and the possibility to print on 3D structures (Mette et al. 2007; Neotech 2021) or even to bond multiple chip layers together, replacing wire bonding due to its large stand-off distance of several millimetres between nozzle and substrate (Hedges and Marin 2012).

A new principle for an Aerosol-on-Demand (AoD) jet-printhead is being developed at our institute (Ungerer et al. 2018). In contrast to conventional aerosol printing systems, the atomiser unit consisting of a capillary and a piezo actuator for ultrasonic excitation is directly integrated into the printhead. This eliminates all supply lines, dead volumes in the ink supply and aerosol preparation equipment. With an established sheath gas flow,

<sup>a</sup> <https://orcid.org/0000-0003-2811-785>

aerosol generation occurs only when needed, and aerosol generation can be switched at any time and at high frequency. Thus, a compact system design can be developed that allows printing operation in all spatial directions, broadly tunable nozzle-to-substrate spacing, and jet-on-demand operation (Ungerer 2020).

Computational fluid dynamics (CFD) models are used to simulate the aerosol printing process and to design the printhead (Sieber et al. 2022; Ungerer 2022). A key issue for stable operation is the accurate positioning of the atomiser unit in the printhead. In this paper, fluid dynamic simulations regarding the positioning of the atomiser unit in the printhead are presented and the results are discussed. Assembly rules, ensuring robust operation, can then be derived from these simulations.

This paper is organised as follows: Section 2 presents the principle set-up of the AoD jet-printhead, in Section 3, a model simplification which is used for the CFD calculation of the influences of the position variation of the atomiser unit is presented. Section 4 shows the simulation results for the individual position tolerances *axial misalignment* and *tilt*. Section 5 deals with the discussion of the results and Section 6 will close the paper with conclusions.

## 2 SET-UP OF THE AoD JET-PRINTHEAD

The AoD jet-printhead consists of the following components: the atomiser unit (consisting of a capillary and piezo actuator), where the aerosol is generated by ultrasonic atomisation, the antechamber, in which the flow homogenisation of the sheath gas takes place, the mixing chamber, in which the incoming sheath gas meets the generated aerosol, and the nozzle, which focuses the aerosol together with the mass flow of the sheath gas. Fig. 1

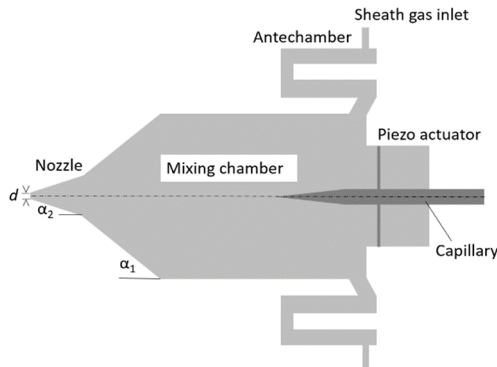


Figure 1: Schematic of the principle design.

shows the schematic of the principle design of the inner contour of the aerosol print head.

Design for manufacturing of the AoD jet-printhead is described in Ungerer et al. 2022, the parameters resulting from this design are summarised in Table 1.

Table 1: Design parameters of the fabrication process (Ungerer et al. 2022).

Parameter	Value
Nozzle angle $\alpha_1$ [°]	45
Nozzle angle $\alpha_2$ [°]	15
Nozzle exit diameter $d$ [mm]	1

As material for the print head, the aluminum alloy AlMgSi1 is selected.

## 3 MODELLING OF THE AoD JET-PRINTHEAD

The modelling of the AoD printhead is based on CFD, a numerical technique for solving fluid dynamics problems. We use Ansys Fluent version R20.1 as the CFD tool for modelling and simulation.

For our modelling approach, we have chosen the Reynolds-averaged Navier-Stokes (RANS) equations (Eqs. 1, 2).

$$\frac{\partial \rho}{\partial t} + \frac{\partial}{\partial x_i} (\rho u_i) = 0 \quad (1)$$

$$\begin{aligned} & \frac{\partial}{\partial t} (\rho u_i) + \frac{\partial}{\partial x_j} (\rho u_i u_j) = \\ & - \frac{\partial p}{\partial x_i} + \frac{\partial}{\partial x_j} \left[ \mu \left( \frac{\partial u_i}{\partial x_j} + \frac{\partial u_j}{\partial x_i} - \frac{2}{3} \delta_{ij} \frac{\partial u_k}{\partial x_k} \right) \right] + \\ & \frac{\partial}{\partial x_j} (-\rho \overline{u_i u_j}) \end{aligned} \quad (2)$$

The continuity equation, which describes the conservation of mass, is described by Eq. 1.  $\rho$  is the density and  $u_i$  is the mean velocity. Eq. 2 represents the conservation of momentum, where  $p$  is the static pressure and the symbol  $\delta_{ij}$  denotes the Kronecker-Delta. To account for turbulence, we use the  $k-\omega$ - $SST$  (shear stress transport) model, a compressible turbulence model, where  $k$  denotes the kinetic energy of the turbulence and  $\omega$  the specific dissipation rate. The calculation of the particle (droplet) tracks follows the Euler-Lagrange approach, where the liquid phase is treated as a continuum by solving the RANS equations, while the dispersed phase is solved by tracking a large number of particles through the calculated flow field of the continuous phase. A more detailed discussion of the equations used in our approach can be found in (Sieber et al. 2022 and

Ungerer et al. 2022). In addition, the interested reader is referred to Wilcox (2006) and Menter (1994) for detailed information on the calculation of these parameters.

Using the RANS equation is generally favourable in terms of computational effort and time, and is thus very suitable for the calculation of complex turbulent flows (Ansys 2021). A wide range of engineering applications can be modelled based on the RANS equations.

Fig. 2 shows the meshed geometry model of the printhead. The mesh was optimised using a mesh independence study resulting in  $2.1 \cdot 10^6$  elements. The meshing of the printhead (left part in Fig. 2) is performed with hexagonal elements. The density of the mesh is controlled in a way that at the inflation layers, forming the mesh near the walls, the element size was  $80 \mu\text{m}$  and in the region between the capillary and the nozzle exit, an element size of  $33 \mu\text{m}$  is achieved to obtain improved resolution in the atomisation region. The free space (right part in Fig. 2) is finely meshed in its centre to obtain a high resolution of the free jet. Outwardly, the meshing is done with larger elements. This mainly controls the number of elements in order to limit simulation time.

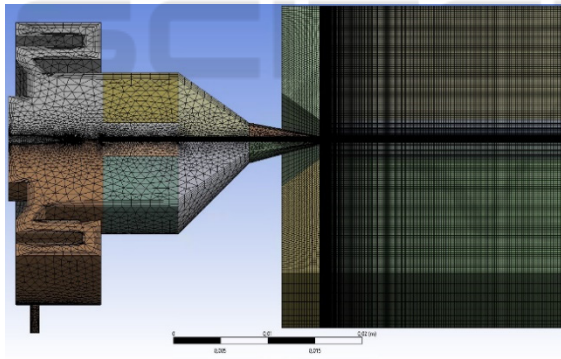


Figure 2: Meshed geometry model of the printhead.

### 3.1 Modelling of the Atomiser Unit

Modelling the ink, the Euler-Lagrange model is used which involves a particle-related consideration of the discrete phase.

The ink itself is modelled as distilled water so that the discrete phase consists of atomised droplets. Replacing the functional ink with distilled water in the model is permissible because aerodynamic focusing does not depend on the dynamic viscosity of the ink or the particle content in the ink. The generated aerosol is modelled in Fluent using a cone model (see Fig. 3), which means the generated aerosol is described by its origin, the cone axis, the

cone angle, radius, diameter of droplets, diameter distribution, exit velocity of the droplets, and aerosol mass flow.

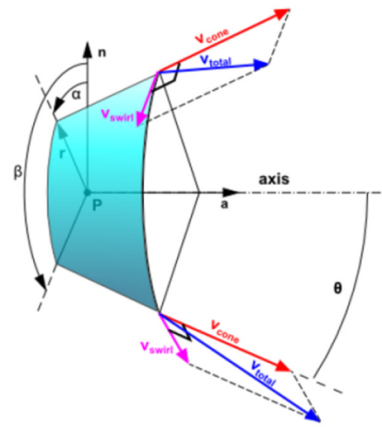


Figure 3: Ansys Fluent cone model (Ansys 2021).

The parameters used for modelling the aerosol source are depicted in Tab. 2.

Table 2: Simulation parameters of the aerosol.

Parameter		Value
origin	[mm]	(17.5/0/0)
cone axis		(1,0,0)
cone angle	[°]	25
radius	[ $\mu\text{m}$ ]	30
max. diameter of droplets	[ $\mu\text{m}$ ]	20
max. exit velocity	[m/s]	10
max. aerosol mass flow	[kg/s]	$1.21 \cdot 10^{-5}$

### 3.2 Simplification of the CFD-Model

In the following position analysis, the influence of the capillary position on the aerosol jet is investigated. To set a certain alignment value of the capillary, the position of the (physical) capillary in the geometry model must be changed each time. In a next step, the meshing has to be adapted to the new geometry. In order to reduce this high modelling effort, we analyse in preliminary investigations whether it is mandatory to model the capillary in the geometry model. The assumption is that the geometry modelling of the capillary can be omitted, since it lies upstream with respect to the flow of sheath gas and aerosol. If this simplified CFD model can be used for the positioning calculations, the alignment investigation is simplified to the adjustment of the parameters of the cone model and the recalculation of the mesh in the changed area.

To analyse whether this simplification is justified, we performed simulations of the velocity distribution of the discrete phase (droplet jet) and the jet diameter

in the free space at different distances from the nozzle exit. In each case, these simulations were performed with and without the geometric modelling of the capillary.

Fig. 4 shows the velocity distribution of the droplet tracks in a representation in which the computational mesh is also shown: top of Fig. 4 shows the droplet tracks with modelled capillary, in the lower representation the capillary is not modelled. The velocity range as well as the velocity distribution over the streamlines are in good agreement between both models. Also, the focusing of the streamlines matches well.

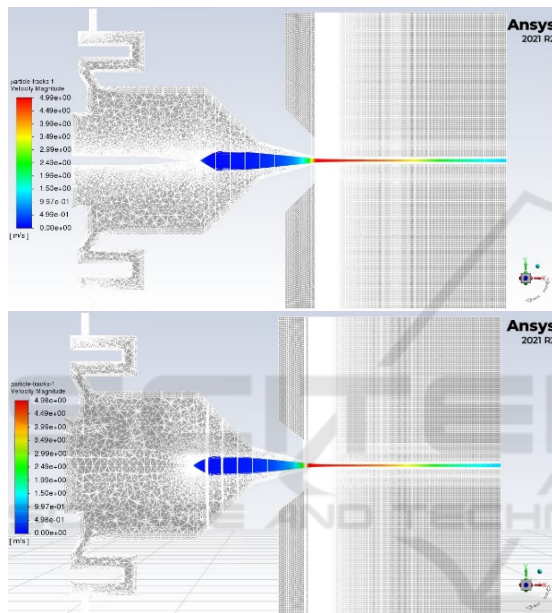


Figure 4: Velocity distribution of droplet tracks with modelled capillary (top) and without modelling the capillary (bottom).

Fig. 5 shows the contour plots of the flow field, also top with the modelled capillary and bottom without. In the contour plots a good qualitative agreement between the flow fields with and without capillary can also be observed. The velocity range of the flow fields are also in good agreement.

A quantitative representation of the droplet velocity is shown in Tab. 3 at two distances to the nozzle exit: 1 mm and 23 mm. Again, the results are depicted for the modelled capillary and without modelling the capillary. In both distances to the nozzle exit the velocity values correspond very well.

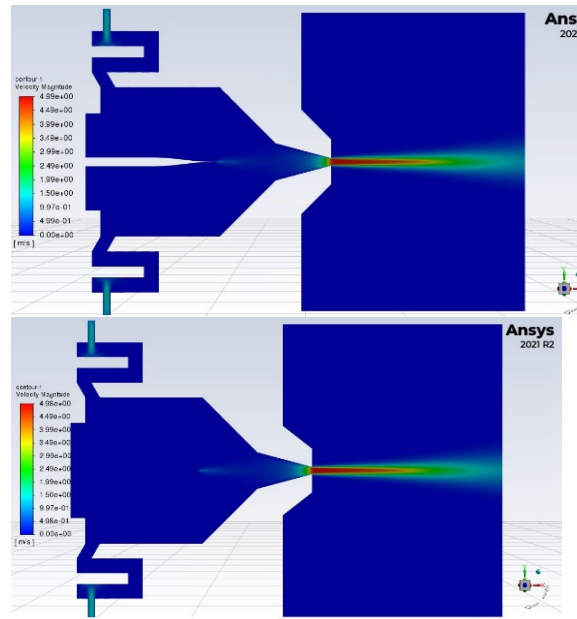


Figure 5: Contour plots of the flow field with modelled capillary (top) and without (bottom).

Table 3: Velocities of the discrete phase at 1 mm and 23 mm distance to nozzle with and without modelled capillary.

	Distance to nozzle exit 1 mm	Distance to nozzle exit 23 mm
With capillary	4,97 m/s	1,52 m/s
Without capillary	4,97 m/s	1,52 m/s

To determine the jet diameters, planes perpendicular to the propagation direction of the jet are placed in the model at defined distances from the nozzle exit. At this positions the concentration of the discrete phase (droplets in the example) is determined. This procedure is excellent for gaining an impression of the jet width at these positions. However, since a different meshing was chosen for the two models with and without capillary (due to the different geometric model) and the evaluation takes place at the nodes of the elements, a direct transfer of the individual concentrations in both plots may differ. However, this does not affect the general statement about the jet widths.

The concentration of the droplets is determined in planes at different distances from the nozzle outlet; Fig. 6 and Fig. 7 show the droplet concentrations at distances of 2 mm and 15 mm from the nozzle outlet, respectively. Fig. 6 shows the distribution of the droplet concentration for the geometry model with capillary. Fig. 7 shows the corresponding for the model without capillary.

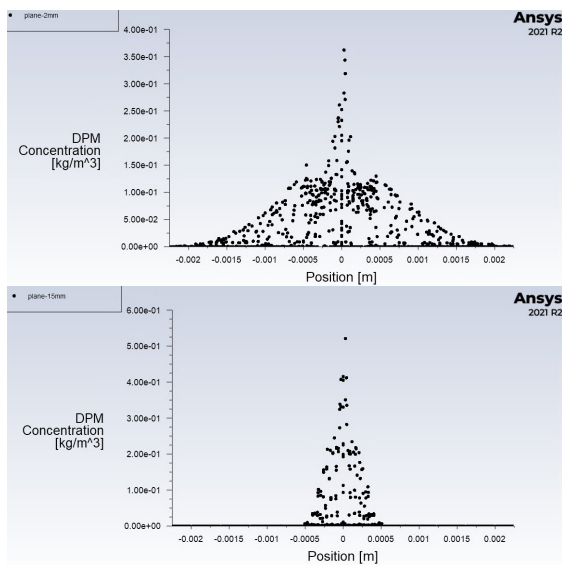


Figure 6: Droplet concentrations as a function of distance to cone axis with capillary. 2 mm distance to nozzle exit (top), 15 mm distance to nozzle (bottom).

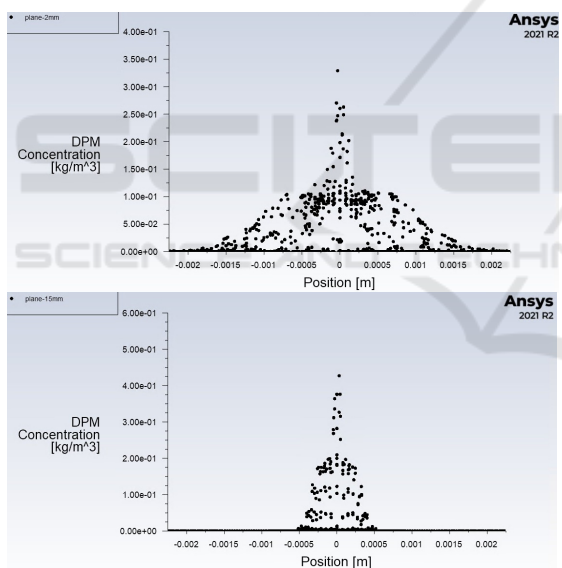


Figure 7: Droplet concentrations as a function of distance to the cone axis without capillary. 2 mm distance to nozzle exit (top), 15 mm to nozzle distance (bottom).

Comparing Fig. 6 with Fig. 7 where the distribution of droplet concentration is depicted in case of the model without cavity, we find them in very good agreement.

In summary, the model simplification by omitting the geometric modelling of the capillary, describes the flow behaviour of the discrete and the continuous phase sufficiently well. Thus, the alignment

simulations can be carried out with this simplified model.

## 4 POSITION ANALYSIS

In order to investigate the influence of the positioning of the atomiser unit in the printhead, simulations of aerosol generation and focusing are carried out for different position variants of the atomiser unit. The two most important alignment parameters are axial alignment and tilting of the atomiser unit within the printhead. In order to evaluate the functionality of the AoD jet-printhead as a function of the positioning of the atomiser unit, the most important criterion is that there is no contact of the aerosol with the inner wall of the nozzle. Such wall contact would not only result in contamination of the inner wall, but could also lead to clogging of the nozzle outlet and consequent collapse of the printing process, or to subsequent dripping of the ink running down the inner wall and consequent destruction of the printed image. Another criterion is that a comparable jet width is achieved to ensure a defined print image.

The influences of these two alignments are discussed in the following two sections.

### 4.1 Axial Alignment of the Atomiser Unit

To model the axial origin displacement of the aerosol, the calculation mesh must be adapted. This is done by shifting a reference plane in the geometry model and a subsequent, automatic remeshing. By adjusting the mesh via the geometry change using the reference plane, a fine mesh in the aerosol origin is ensured. Furthermore, it is ensured that the mesh in the nozzle interior is always generated identically in the core, so that a comparison can be made in the front nozzle interior independent of the mesh. Likewise, the entire mesh in the free space is independent of the aerosol origin and always identical.

Positions at 2 mm intervals in the range [9.5 mm, 23.5 mm] are examined. The position of the piezo actuator serves as reference (see Fig. 1). For all positions inside the defined range no wall contact was observed, hence the most important criterion for successful printing is fulfilled.

Figure 8 shows the velocity distributions of the droplet tracks for the two extreme positions (9.5 mm and 23.5 mm) and the position 15.5 mm.

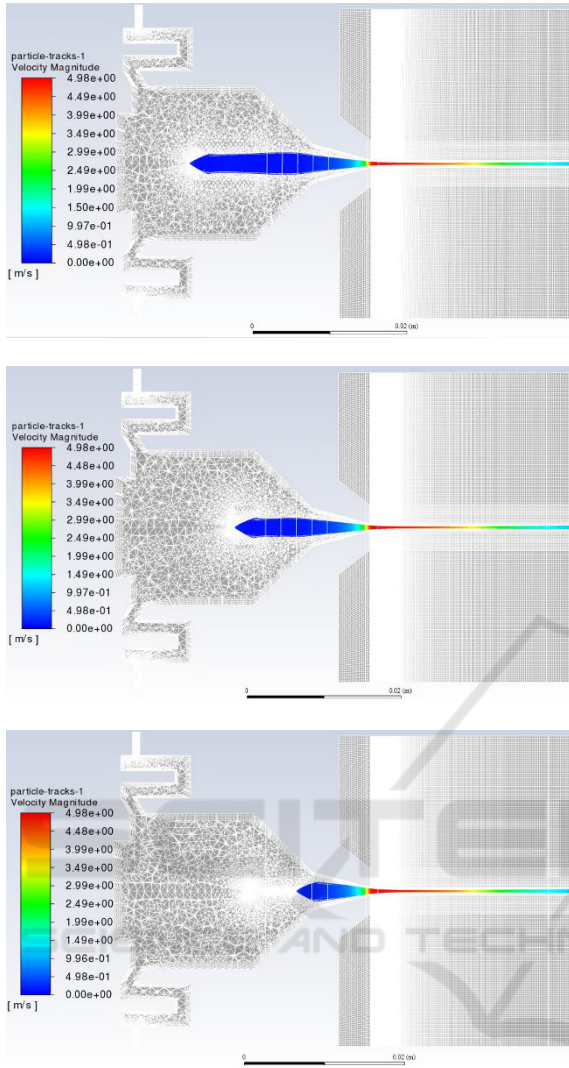


Figure 8: Velocity distribution of droplet tracks for different axial alignments: 9.5 mm, 15.5 mm and 23.5 mm (from top to bottom).

An examination of the velocity distributions of the droplet tracks for the different axial positions of the atomiser unit yields comparable velocity values and also droplet curves. Of particular interest are the droplet tracks in the free space: here, both the velocities and the jet widths are independent of the axial positioning of the atomiser unit.

Hence, the printhead system, as it is set up, is very robust with regard to an axial positioning of the atomiser unit.

### 4.2 Tilting of the Atomiser Unit

Since the tilts of the cone axis do not cause any changes in the mesh, there is no need to modify the

computational mesh depending on the angle of inclination of the aerosol origin.

In the description of the aerosol source (see Tab. 1), a tilting of the capillary in the atomizer unit leads on the one hand to a change in the orientation of the *cone axis* and on the other hand to a displacement of the *origin* (see Fig. 9). The values of the considered tilt angles and the corresponding offset values are shown in Tab. 4.

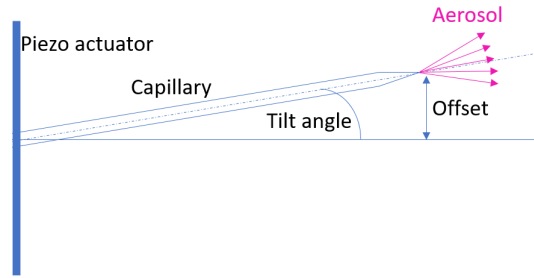


Figure 9: Capillary tilt of the atomiser unit.

Table 4: Tilt angles and corresponding offset values.

Tilt [°]	0.21	0.42	0.64	0.85	1.06
Offset [mm]	0.05	0.1	0.15	0.2	0.25
Tilt [°]	1.27	1.70	2.12	4.25	8.52
Offset [mm]	0.3	0.4	0.5	1.0	2.0

Figure 10 shows the velocity distributions of the droplet tracks for tilt angles of 0.21°, 1.06°, 4.25°, and 8.52°. In the sequence of simulation results from Fig. 10 a) to d), the deflection of the aerosol source and the associated skew propagation of the droplets within the nozzle can be clearly seen. In all the cases shown, the inflowing sheath gas, together with the contour of the nozzle, achieves a focusing of the aerosol jet at the nozzle outlet. For larger angles (see Fig. 10 c) and d)), it can be seen that the aerosol jet does not emerge from the center of the nozzle, but has an offset. The velocity profile of the jet in the free space remains relatively stable as a function of the tilt, but a slightly increased velocity magnitude is observed for larger tilt angles (accompanied by a larger offset of the source origin).

The simulations of all investigated tilts and their corresponding offsets show no wall contact, which is defined by an exit condition of the droplets. Again, the most important criterion for successful printing is fulfilled. However, from a tilting angle of 4.25° and the associated offset of 1 mm, droplets are also found in the outermost mesh elements close to the wall, so that possible wall contact cannot be fully ruled out here (see Fig. 10 c)

and d)). A stable focusing behavior can be assumed for capillary tilts of less than approx.  $2^\circ$ .

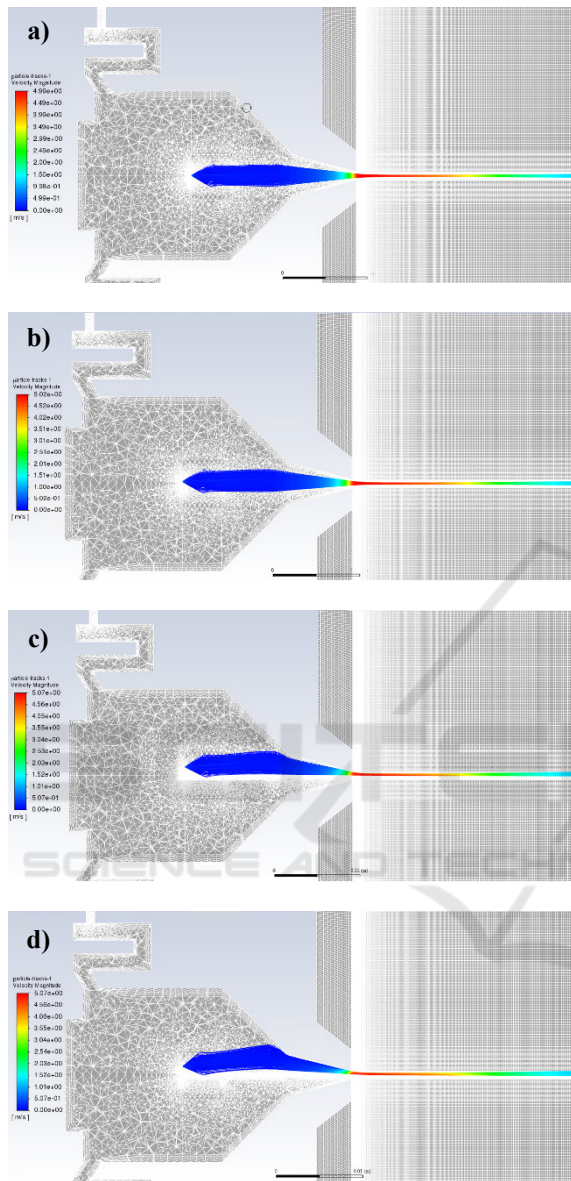


Figure 10: Velocity distributions of the droplet tracks for tilt angles of  $0.21^\circ$  (a),  $1.06^\circ$  (b),  $4.25^\circ$  (c), and  $8.52^\circ$  (d) and corresponding offsets.

## 5 RESULTS AND DISCUSSION

A key issue for stable operation of the AoD is the accurate positioning of the atomiser unit in the printhead. To investigate the sensitivity of the operation in this respect, analysis of the positioning of the atomiser unit in the printhead are conducted for

axial misalignment as well as for a tilt of the atomiser unit. Analysis of the axial positioning of the atomiser unit shows that operation of the printhead is very robust with respect to axial positioning. No influence on the droplet tracks can be observed: both the velocity variations within the tracks and the jet widths show no effects with respect to the axial orientation of the aerosol source in the investigated range [9.5 mm, 23.5 mm]. Regarding the axial positioning, we can state that the setup used is very robust.

Analysing the tilt of the atomiser unit, both the tilt angle and the offset of the aerosol source from the origin are considered. The simulations of the tilt angles show no direct wall contact for an angle range up to  $8.52^\circ$ . However, since the droplet tracks are within the outermost mesh elements towards the wall for angles larger than  $4.25^\circ$ , a possible wall contact cannot be completely excluded here. Furthermore, it can be observed that for larger tilts, the focused aerosol jet leaves the nozzle exit not in the center, but under an offset. From this it can be concluded that stable focusing with regard to tilting of the atomiser unit is achieved for angles smaller than  $2^\circ$ . Due to this sensitivity of the operation with regard to tilting of the atomizing unit, the tilt must be controlled during assembly.

## 6 CONCLUSIONS

In this article, the influence of the atomiser unit alignment of an Aerosol-on-demand jet-printhead for functional printing is presented using CFD simulations. Two relevant alignment parameters are investigated in this article, namely axial alignment and tilting of the atomiser unit. In order to simplify the simulation procedure, it is shown in a first step that the capillary as a physical unit does not have to be represented in the model. This avoids the need to change the position of the (physical) capillary in the geometry model for each alignment value of the capillary and subsequently to adapt the meshing to the new geometry.

Based on this simplified model, the effects of the atomiser unit alignment on the droplet tracks are determined. The velocity profiles and the focusing of the aerosol jet within the nozzle and in the free space are evaluated.

Two conditions must be met for the reliable function of the AoD jet-printhead:

1. generation of a stable and focused aerosol jet
2. prevention of wetting of the inner nozzle wall by the aerosol.

Under these conditions, our analysis shows that the setup is robust with respect to the axial positioning of the atomizer unit. In terms of inclination, we have found that a tilt of up to 2° is tolerable, but inclinations beyond this should be prevented by suitable mounting methods.

The results of this work will be used to derive rules for the assembly and installation of the atomiser unit in the AoD jet-printhead.

## ACKNOWLEDGEMENTS

The authors would like to acknowledge Achim Wenka (IMVT, KIT) for his continuing support in the field of computational fluid dynamics and Klaus-Martin Reichert (IAI, KIT) for soft- and hardware support.

## REFERENCES

- Ansys 2021. *Ansys Fluent User's Guide, Release 2021 R2*, ANSYS, Inc. Canonsburg, PA, USA
- Cui, Z. 2016. Printed electronics - Materials, Technologies and Applications. *John Wiley & Sons, Singapore*. ISBN: 9781118920954
- Dyson, M. 2022. *3D Electronics/Additive Electronics 2022-2032*, Research Report. IDTechEx Ltd.
- Ganz, S., H.M. Sauer, S. Weißenseel, J. Zembron, R. Tone, E. Dörsam, M. Schaefer, M. Schulz-Ruthenberg. 2016. *Printing and Processing Techniques*. Nisato, G., Lupo, D., and Ganz, S. (editors): *Organic and Printed Electronics: Fundamentals and Applications*: 48-116. Singapore: Pan Stanford Publishing.
- Gengenbach, U., M. Ungerer, L. Koker, K.-M. Reichert, P. Stiller, S. Allgeier, B. Köhler, X. Zhu, C. Huang and V. Hagenmeyer. 2020. Automated fabrication of hybrid printed electronic circuits. *Mechatronics* 70. 102403. DOI: 10.1016/j.mechatronics.2020.102403
- Gupta, A.A., A. Bolduc, S. G. Cloutier and R. Izquierdo. 2016. Aerosol Jet Printing for printed electronics rapid prototyping, *IEEE International Symposium on Circuits and Systems (ISCAS), Montreal, QC*: 866-869, doi: 10.1109/ISCAS.2016.7527378.
- Hedges, M. and A. B. Marin. 3D Aerosol Jet Printing - Adding Electronics Functionality to RP/RM. *Direct Digital Manufacturing Conference (Berlin) 2012*. url: [https://www.optomec.com/wp-content/uploads/2014/04/Optomec\\_NEOTECH\\_DDMC\\_3D\\_Aerosol\\_Jet\\_Printing.pdf](https://www.optomec.com/wp-content/uploads/2014/04/Optomec_NEOTECH_DDMC_3D_Aerosol_Jet_Printing.pdf). (accessed: 23.05.2023).
- Kwon, K.-S., Md. K. Rahman; T. H. Phung, S. D. Hoath, S. Jeong, J. S. Kim. 2020. Review of digital printing technologies for electronic materials. *Flex. Print. Electron.* 5. 043003. DOI: 10.1088/2058-8585/abc8ca.
- Magdassi, S. 2010. *The Chemistry of Inkjet Inks*. Singapore: World Scientific Publishing.
- Menter, F.R. 1994. Two-Equation Eddy-Viscosity Turbulence Models for Engineering Applications. *AIAA Journal*. 32(8): 1598-1605.
- Mette, A., P. L. Richter, M. Hörteis, S. W. Glunz. 2007. Metal Aerosol Jet Printing for Solar Cell Metallization, *Progress in Photovoltaics* 15, 621-627. doi: 10.1002/pip.759.
- Neotech. 2021. 3D Printed Electronics applications realised by Neotech AMT. url: <https://neotech-amt.com/applications>. (accessed: 23.05.2023).
- Oakley, C and P. Chahal. 2018. Aerosol Jet Printed Quasi-Optical Terahertz Components. *IEEE Trans. THz Sci. Technol.* vol. 8, no. 6, pp. 765-772. DOI: 10.1109/TTHZ.2018.2873915
- Schlichting, H. and K. Gersten. 2006. *Grenzschichttheorie*. 10. Auflage. Berlin, Heidelberg: Springer. doi: 10.1007/3-540-32985-4.
- Sieber, I. R. Thelen, and U. Gengenbach. 2020. Assessment of high-resolution 3D printed optics for the use case of rotation optics. *Opt. Express* 28: 13423-13431.
- Sieber, I., R. Thelen, and U. Gengenbach. 2021. Enhancement of High-Resolution 3D Inkjet-printing of Optical Freeform Surfaces Using Digital Twins. *Micromachines* 12(1): 35. <https://doi.org/10.3390/mi12010035>.
- Sieber, I., Zeltner, D., Ungerer, M., Wenka, A., Walter, T., Gengenbach, U. (2022). Design and experimental setup of a new concept of an aerosol-on-demand print head. *Aerosol Science and Technology*. Taylor & Francis. DOI: 10.1080/02786826.2021.2022094
- Sirringhaus, H. and T. Shimoda. 2003. Inkjet Printing of Functional Materials. *MRS Bulletin* 28(11): 802-806. doi: 10.1557/mrs2003.228.
- Ungerer, M., A. Hofmann, R. Scharnowell, U. Gengenbach, I. Sieber, and A. Wenka. 2018. Druckkopf und Druckverfahren [Print head and printing method]. Patent: DE 10 2018 103 049.5.
- Ungerer, M. 2020. Neue Methodik zur Optimierung von Druckverfahren für die Herstellung funktionaler Mikrostrukturen und hybrider elektronischer Schaltungen [New methodology for optimising printing processes for the production of functional microstructures and hybrid electronic circuits]. Dissertation, Karlsruhe, Germany: Karlsruhe Institute of Technology (KIT).
- Ungerer, M.; Zeltner, D.; Wenka, A.; Gengenbach, U. and Sieber, I. 2022. Modelling and Simulation of an Aerosol-on-Demand Print Head with Computational Fluid Dynamics. In *Proceedings of the 12th International Conference on Simulation and Modeling Methodologies, Technologies and Applications*, 44-51. DOI: 10.5220/0011258100003274
- Wilcox, D.C. 2006. *Turbulence Modelling for CFD*, 3rd edition). La Canada, California: DCW Industries, Inc.
- Zikulnig, J., S. Chang, J. Bito, L. Rauter, A. Roshanghias, S. Carrara, and J. Kosel. 2023. Printed Electronics Technologies for Additive Manufacturing of Hybrid Electronic Sensor Systems. *Adv. Sensor Res.* 2200073, doi: 10.1002/adsr.202200073.